Chemistry & Biology
Article

TR-FRET-Based Duplex Immunoassay Reveals an Inverse Correlation of Soluble and Aggregated Mutant huntingtin in Huntington's Disease

Barbara Baldo,[1,4] Paolo Paganetti,[1,4,5] Stephan Grueninger,[1] David Marcellin,[1] Linda S. Kaltenbach,[2] Donald C. Lo,[2] Martin Semmelroth,[1] Andjelija Zivanovic,[1] Dorothée Abramowski,[1] Donna Smith,[3] Gregor P. Lotz,[1] Gillian P. Bates,[3] and Andreas Weiss[1,*]

[1]Neuroscience Discovery, Novartis Institutes for BioMedical Research, Basel CH-4002, Switzerland
[2]Center for Drug Discovery and Department of Neurobiology, Duke University Medical Center, Durham, NC 27705, USA
[3]Department of Medical and Molecular Genetics, King's College London, London SE1 8WA, UK
[4]These authors contributed equally to this work
[5]Present address: AC Immune SA, Lausanne 1015, Switzerland
*Correspondence: andreas-1.weiss@novartis.com
DOI 10.1016/j.chembiol.2011.12.020

SUMMARY

Huntington's disease (HD) is an inherited neurodegenerative disorder caused by the amplification of a polyglutamine stretch at the N terminus of the huntingtin protein. N-terminal fragments of the mutant huntingtin (mHtt) aggregate and form intracellular inclusions in brain and peripheral tissues. Aggregates are an important hallmark of the disease, translating into a high need to quantify them in vitro and in vivo. We developed a one-step TR-FRET-based immunoassay to quantify soluble and aggregated mHtt in cell and tissue homogenates. Strikingly, quantification revealed a decrease of soluble mHtt correlating with an increase of aggregated protein in primary neuronal cell cultures, transgenic R6/2, and *Hdh*Q150 knock-in HD mice. These results emphasize the assay's efficiency for highly sensitive and quantitative detection of soluble and aggregated mHtt and its application in high-throughput screening and characterization of HD models.

INTRODUCTION

Huntington's disease (HD) is an autosomal dominant neurodegenerative disease caused by the amplification of a polyglutamine (polyQ) stretch at the N-terminus of the huntingtin protein (Htt) (The Huntington's Disease Collaborative Research Group, 1993). N-terminal fragments of mutant Htt (mHtt) are generated by proteolytic cleavage and acquire a misfolded conformation through the polyQ stretch, leading to the formation of nuclear and cytoplasmic aggregates (Hazeki et al., 1999; Landles et al., 2010; Lunkes et al., 2002; Wang et al., 2008).

HD is characterized by progressive deposition of these insoluble aggregates involving the formation of intermediate states (fibrils and oligomers), whose precise composition and structure is still under investigation (Hoffner et al., 2005; Legleiter et al., 2010; Ratovitski et al., 2009). Whether the aggregates have a toxic role is still controversial (Gutekunst et al., 1999; Kuemmerle et al., 1999; Wanker, 2000), but the correlation between disease status and aggregate load found in postmortem brains from HD patients highlights the importance to quantify their formation (DiFiglia et al., 1997; Gutekunst et al., 1999; Maat-Schieman et al., 1999).

When expressed in mice, mHtt is highly pathogenic. For instance, R6/2 mice express an Exon1 mHtt fragment with ~200 polyQ and develop an aggressive form of the disease with strong aggregation in the brain and peripheral tissues (Mangiarini et al., 1996; Stack et al., 2005). *Hdh*Q150 knock-in mice, generated by introducing 150 polyQ in the endogenous Htt gene, show slower aggregate formation and disease progression (Sathasivam et al., 2010; Woodman et al., 2007).

In order to evaluate a treatment effect on the modulation of aggregate load and to better characterize the role of aggregated and soluble mHtt in the disease, sensitive and quantitative detection methods for different forms of mHtt are essential. Currently mHtt aggregate determination involves labor-intensive biochemical techniques (filter trap or AGERA [Wanker et al., 1999; Weiss et al., 2008]), a Seprion ligand based ELISA (Sathasivam et al., 2010), or immunohistochemistry assays which are often semiquantitative, therefore not sensitive enough to detect small variations (Hazeki et al., 2002; Mitsui et al., 2006).

In this study, we combined the advantages of a time-resolved Förster resonance energy transfer (TR-FRET) assay (sensitivity, robustness, speed, usage of small volumes and duplexing potential) with the principle of using a single monoclonal antibody for detection of aggregated mHtt, as shown for ELISA-based detection of multimeric α-synuclein or amyloid-β peptide in human samples (El-Agnaf et al., 2006; Fukumoto et al., 2010). TR-FRET immunoassay detection is based on the labeling of an antibody pair with a rare earth ion fluorophore donor and an acceptor fluorophore. Due to the rare earth ion large Förster's distance of ~9 nm (Mathis, 1993), an energy transfer between the two fluorophores can occur over great distances, thereby producing a specific TR-FRET signal when the donor and acceptor labeled antibodies bind to their antigen simultaneously. The development of this new technology enables the

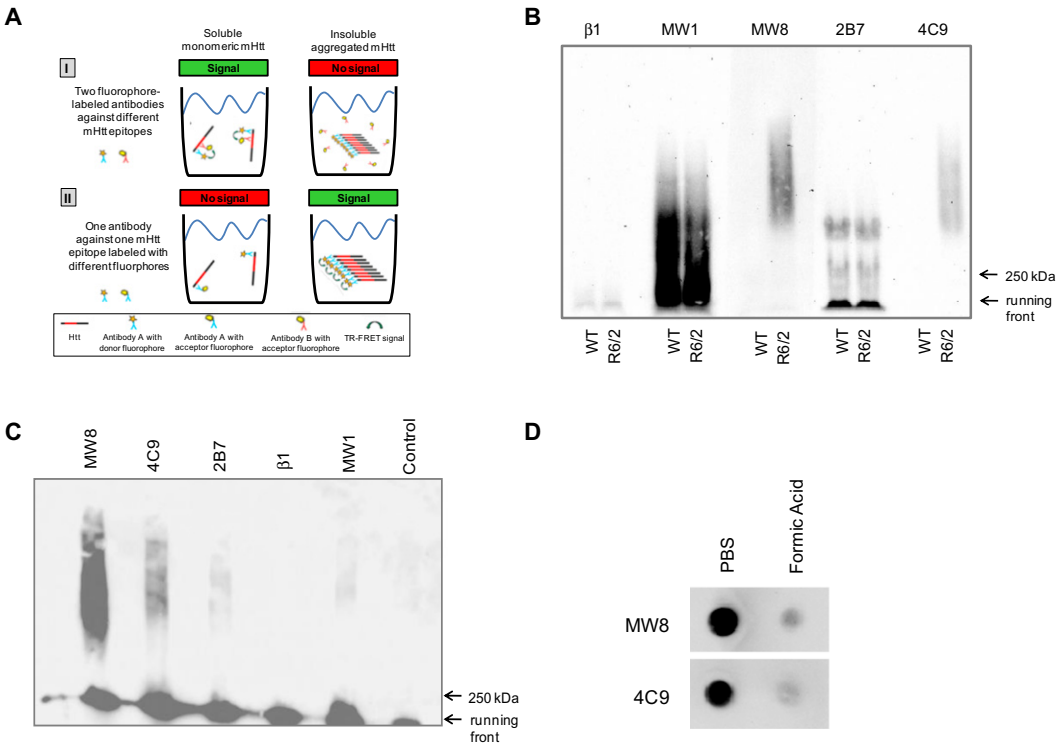

Figure 1. Htt Antibodies Detect mHtt Aggregates with Different Affinities

(A) Representation of the principle behind Htt-aggregate detection by TR-FRET. Soluble mHtt protein can be recognized using two antibodies A and B directed against different, sterically unblocked epitopes. The close proximity of donor (A) and acceptor (B) fluorophores results in a TR-FRET signal in this state (I, left box). When mHtt protein forms insoluble aggregates, only antibody A recognizes it, as the specific epitope is still sterically unblocked. In contrast, antibody B, which is directed against the expanded polyQ-stretch (red region in Htt-exon1 protein) can no longer bind. Under these conditions, A and B are not in close enough proximity to result in a signal (I, right box). On the contrary, a mixture of antibody A labeled with either donor or acceptor fluorophore results in a TR-FRET signal for aggregated (II, right box) but not soluble Htt (II, left box).

(B) High molecular weight mHtt aggregates in brain homogenates of 12-week-old WT or R6/2 mice are specifically detected by MW8 and 4C9 antibodies on an AGERA blot. MW1 antibody shows an unspecific signal in both WT and R6/2 brains. Similar to β1, an amyloid-beta specific control antibody, 2B7 antibody does not detect mHtt aggregates from R6/2 brain.

(C) mHtt aggregates were successfully immunoprecipitated with 4C9 and MW8 antibody, only weakly with 2B7 and MW1, but not with β1 or the control (G-Sepharose beads). Samples were resolved on AGERA blot and detected with MW8.

(D) Filter trap assay on the brain homogenates of 8-week-old R6/2 mice. mHtt aggregates are specifically detected by 4C9 and MW8 antibodies after re-suspension in PBS. No signal is detectable when mHtt aggregates are dissolved by treatment with formic acid.

See also Figure S1.

simultaneous quantification of small variations in mHtt aggregate load during disease progression in comparison to changes affecting the soluble pool of the mutant protein. Next to its application for characterizing HD models, due to its sensitivity and simplicity, the method is also applicable to high-throughput screenings to evaluate modifiers of disease progression.

RESULTS

huntingtin Antibodies Detect High Molecular Weight Aggregates with Different Specificity

We have recently reported a TR-FRET-based immunoassay for the detection of soluble mHtt species in cell lysates and tissue homogenates (Weiss et al., 2009; Weiss et al., 2011). The first question we addressed is whether we could detect large mHtt aggregates using the same technology, but with aggregate-specific antibodies. The combination of both detection systems for soluble and aggregated mHtt would allow us to track the protein aggregation over time in biological samples.

The assay for soluble mHtt uses two labeled monoclonal antibodies directed toward proximal N-terminal epitopes. One of the antibodies, MW1, is specific for the elongated polyQ stretch through which mHtt aggregates. The epitope would therefore be masked in the presence of mHtt aggregates, resulting in loss of TR-FRET signal (Figure 1A, upper panel). In contrast, mHtt aggregates will present multiple binding sites for one single antibody in close proximity. This would allow simultaneous binding of the monoclonal antibody labeled with donor and acceptor fluorophores and thus generation of a TR-FRET signal (Figure 1A, lower panel).

The first challenge, therefore, was to find the right antibodies for a TR-FRET-based assay specific and selective for mHtt aggregate detection (antibodies used in this study are presented in Figure S1 available online). We first performed AGERA blotting

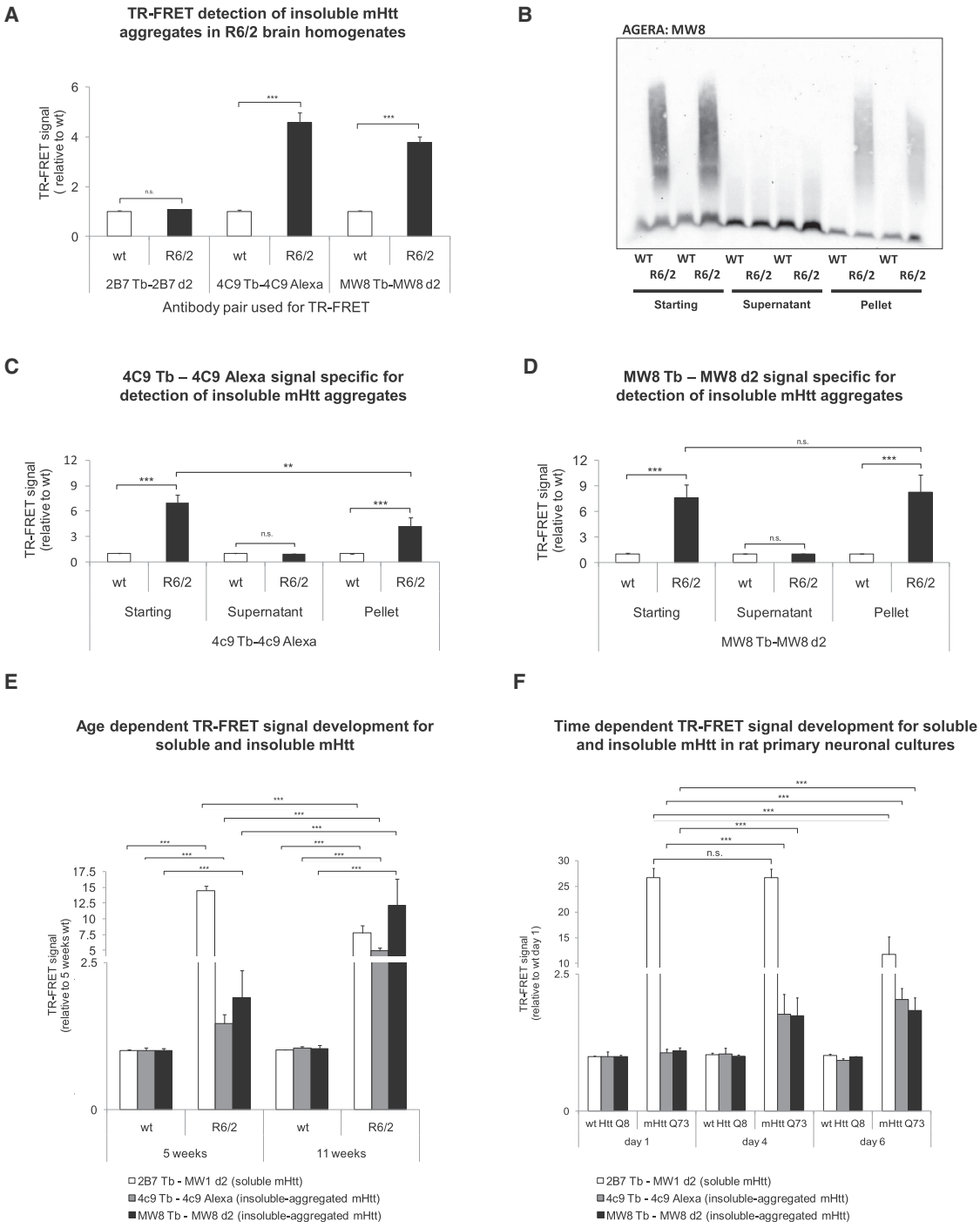

Figure 2. Antibody Pairs Expected to Detect mHtt Aggregates Work for TR-FRET

(A) TR-FRET assay on brain homogenates of 12-week-old WT or R6/2 with a mixture of one mHtt antibody labeled with either donor or acceptor fluorophore. Antibodies 4C9 or MW8 detect an mHtt-specific signal in R6/2 mouse brains, whereas 2B7 fails to detect TR-FRET signal (n = 3, 0.5 μg protein loaded per 384-well).

(B) Brain homogenates of 12-week-old WT or R6/2 mice (starting fraction) were separated by ultracentrifugation into a soluble (supernatant) and an insoluble (pellet) fraction (n = 2). AGERA blot with MW8 antibody shows that all mHtt aggregates were recovered in the pellet fraction, whereas no mHtt-specific aggregates were found in the supernatant fraction.

(C and D) TR-FRET assay for ultracentrifugation fractions shows that MW8/MW8 and 4C9/4C9 specifically detect insoluble aggregated mHtt but not soluble protein recovered in the supernatant fractions.

(E) Age-dependent increase of insoluble aggregated mHtt in 4- and 12-week-old R6/2 mouse brain homogenates is detected by TR-FRET using MW8/MW8 and 4C9/4C9. In contrast, TR-FRET analysis with 2B7/MW1 reveals a correlating decrease in soluble mHtt over time (n = 3).

using brain homogenates of wild-type (WT) and R6/2 transgenic mice. 4C9 and MW8 antibodies showed specific mHtt aggregate detection in R6/2 when compared to WT homogenates (Figure 1B). In contrast, MW1 and 2B7 antibodies were not aggregate-specific and resulted in a diffuse and mHtt unspecific signal in WT as well as R6/2 samples. Negative control antibody β1 directed against β-amyloid peptide failed to recognize mHtt aggregates.

Because the TR-FRET assay is based on antibody-antigen interactions in solution, we wanted to further validate the specific binding of 4C9 and MW8 to mHtt aggregates by immunoprecipitation. Aggregates were efficiently immunoprecipitated by 4C9 and MW8 but not by 2B7, MW1, and β1 antibodies, confirming the specificity of these two antibodies for high molecular weight complexes of mHtt in solution (Figure 1C). Further proof of the antibodies' specificity for insoluble mHtt aggregates has been obtained by dissolving mHtt aggregates via formic acid treatment. 4C9 and MW8 produced a detectable signal in a filter trap assay for aggregates larger than 200 nm when pelleted mHtt aggregates from 8-week-old R6/2 brains were resuspended in PBS, but failed to produce any signal when the samples were resuspended and treated with formic acid (Figure 1D).

These results indicate that 4C9 as well as MW8 antibodies are mHtt aggregate-specific tools for the development of a TR-FRET-based immunoassay for mHtt aggregates.

TR-FRET Detection of Aggregated mHtt

Having demonstrated that 4C9 and MW8 detect mHtt aggregates by AGERA and immunoprecipitation methods, we proceeded to evaluate whether 4C9 and MW8 could detect mHtt aggregates via TR-FRET, based on our model in Figure 1A. The antibodies were labeled with donor or acceptor fluorophores, respectively Terbium (Tb) and d2 or Alexa488 (Alexa). WT and R6/2 brain homogenates from 12-week-old mice were analyzed with 4C9 Tb-4C9 Alexa (4C9/4C9), MW8 Tb-MW8 d2 (MW8/MW8) and 2B7 Tb-2B7 d2 (2B7/2B7) as a negative control pair. As expected, use of the 2B7/2B7 combination did not result in a mHtt aggregate-specific signal, whereas a significant difference between WT and R6/2 samples was observed with the two antibody combinations MW8/MW8 and 4C9/4C9 (Figure 2A), indicating the specificity of mHtt aggregate detection based on TR-FRET. This specificity was further validated by the absence of TR-FRET signal in samples treated with formic acid to dissolve aggregates (Figure S2).

Additionally, we separated 12–week-old R6/2 mouse brain homogenates into soluble (supernatant) and insoluble (pellet) fractions by ultracentrifugation with a force of 80,000 × *g*. Under this condition, all insoluble aggregates sediment. All aggregates present in the starting fraction were recovered in the pellet fraction as shown by AGERA blot (Figure 2B). This result is concordant with previous results where ultracentrifugation was used to identify different populations of purified tagged mHtt (Olshina et al., 2010). Next, we analyzed the three fractions via TR-FRET. Both the 4C9/4C9 and MW8/MW8 combinations specifically recognized the aggregated mHtt in the starting homogenate and in the pellet fractions, but failed to generate any signal in the supernatant (Figures 2C and 2D). In contrast, 2B7/MW1 combination generates a signal in the starting homogenate and in the supernatant, consistent with the specificity for soluble mHtt (Weiss et al., 2009) (Figure S3A). To investigate the mHtt detection specificity of 2B7/MW1 in more detail, we generated an allelic series of purified soluble Htt protein with increasing polyQ repeat length. Analysis confirmed the recognition of soluble mHtt by the 2B7/MW1 combination with a distinct progressive increase in signal strength correlating with an increasing polyQ with a ~10fold higher sensitivity for polyQ length region found in the mutant allele in over 95% of HD patients (40-55 Q) compared to the normal polyQ length present in the WT protein (16-22Q) (Figures S3B and S3C) (Myers, 2004).

Taken together, these results show that 4C9/4C9 as well as MW8/MW8 assays detect specifically insoluble mHtt aggregates, while 2B7/MW1 antibody combination is specific for soluble mHtt. The results confirm the hypothesis we claimed in our aggregation model (Figure 1A). To our knowledge, this is the first time that a simple one-step assay detects specifically nontagged insoluble mHtt aggregates.

We proceeded to use the new TR-FRET assays to characterize mHtt aggregation in biological samples over time. Previous work shows an inverse correlation between aggregated and soluble mHtt as a function of disease progression in R6/2 mice (Sathasivam et al., 2010; Weiss et al., 2009; Woodman et al., 2007). We therefore asked whether we could confirm this inverse correlation with the TR-FRET technology using antibody combinations for soluble (2B7/MW1) and aggregated mHtt (MW8/MW8 and 4C9/4C9) (Figure 2E). Indeed, analysis of R6/2 mice at disease onset (5 weeks of age) and late manifest state (11 weeks of age) show progressive formation of aggregated mHtt with a correlating decrease of soluble mHtt. This confirmed previous findings and underlined the robustness and specificity of the TR-FRET assay.

Next to its application in tissue samples, we asked whether the mHtt TR-FRET assay can be used in a screening format to quantify untagged mHtt aggregates in neuronal cell cultures. To this aim, we used mHtt exon1-73Q or WT exon1-8Q transiently transfected primary neuronal cortico-striatal cocultures in a 96-well microtiter plate. We monitored mHtt aggregation over time using the TR-FRET assay. Both MW8/MW8 and 4C9/4C9 combination detected aggregated mHtt 4 and 6 days after transfection, accompanied by a decrease of the soluble mHtt 2B7/MW1 signal (Figure 2F). These results demonstrate that the TR-FRET assays allow for monitoring changes of aggregated and soluble untagged mHtt in neuronal cocultures grown in microtiter plates.

We wanted to further verify the specificity of the 2B7/MW1 combination for soluble and 4C9/4C9 or MW8/MW8 for aggregated mHtt by an independent method. We therefore proceeded to resolve different mHtt subpopulations from 4- and 8-week-old R6/2 mouse brains by using size exclusion chromatography

(F) Time-dependent increase of insoluble aggregated mHtt is detected by TR-FRET using the MW8/MW8 and 4C9/4C9 in rat primary striatal-cortical cocultures lysates transiently transfected with exon1-Htt with Q8 or exon1-mHtt with Q73 (n = 6 per condition). TR-FRET analysis with 2B7/MW1 shows a correlating decrease in soluble mHtt over time. Error bars = SD. **p < 0.01; ***p < 0.001. n.s., not significant.
See also Figures S2 and S3 and Table S2.

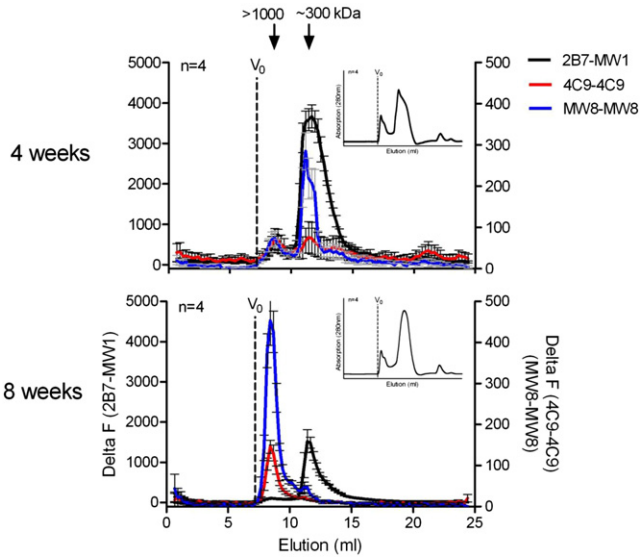

Figure 3. Detection of a Subset of Soluble mHtt Aggregates in R6/2 Brain Lysate at Different Age with a Combination of SEC and TR-FRET

Supernatant obtained from centrifuged R6/2 brain homogenate was loaded onto a Superdex200 column, and the fractions were analyzed by TR-FRET with indicated antibody combination. Graphs show TR-FRET signal profiles of SEC-eluted supernatant of R6/2 brain tissue homogenate at 4 weeks and 8 weeks of age (n = 4 per age). The black lines correspond to the 2B7/MW1 signal profile, the red lines correspond to the 4C9/4C9 signal profile, and the blue lines correspond to the MW8/MW8 TR-FRET signal profile. The small inner graphs indicate the total protein elution profile by UV. Arrows indicate the estimated size of main peaks in kDa by using protein standards in the same running buffer (protein standard data not shown). Error bars = SD.
See also Figure S4.

(SEC) (Lotz et al., 2010) (Figure 3). Analysis of the fractions with 2B7/MW1 TR-FRET combination detected low molecular weight mHtt species of around 300 kDa at 4 weeks of age, which decreased in intensity at 8 weeks of age. In contrast, MW8/MW8 and 4C9/4C9 TR-FRET detected high molecular weight mHtt species around 950 kDa, which increased in intensity at 8 weeks of age. Intriguingly, heterogeneity did not change temporally, but the relative abundance of individual mHtt aggregates did. No mHtt TR-FRET signals were observed when using WT brain homogenates as a control (Figure S4).

Another important observation was that in 4-week-old mice, the MW8/MW8 combination but not the 4C9/4C9 combination detected a subset of low molecular weight mHtt aggregates, partially overlapping with the 2B7/MW1 signal (Figure 3). This result suggests that all three TR-FRET assays recognize different Htt species, where 4C9/4C9 and MW8/MW8 preferentially bind to aggregates and 2B7/MW1 binds to soluble mHtt. Moreover, these results verify the inverse correlation of soluble and aggregated mHtt over time in R6/2 mice and identify specific smaller and larger Htt aggregates that are distinguishable with the different TR-FRET antibody combinations.

We continued to investigate whether we could detect an inverse correlation of these mHtt species during aging in different brain regions. To address this question, we analyzed different brain regions of female and male R6/2 mice at 4, 8, 12, and 15 weeks of age. For both sexes and all brain regions, we observed a consistent age-dependent decrease in soluble mHtt associated with a progressive increase in aggregated mHtt (Figure 4 and Figure S5). No significant differences between genders were found with the exception for soluble mHtt in the cerebellum, which seemed to decrease more slowly in males than in females. In the cerebellum and hippocampus, aggregate deposition was less rapid than in the other brain regions when measured with the MW8/MW8 antibody pair but not with the 4C9/4C9 assay. These findings show that the inverse correlation between soluble and aggregated mHtt found in total brain homogenates also occurs in sub-brain regions.

Duplex TR-FRET Assay for Simultaneous Detection of Soluble and Aggregated mHtt

To further enhance the simplicity of the detection method, we thought to develop a duplex assay that could simultaneously be used to measure both forms of the protein in the same biological sample, following the single pipetting-step procedure depicted in Figure S6 and using two different acceptor fluorophores (d2 and Alexa) coupled to MW1 and 4C9, respectively, which can be simultaneously excited by Tb donors.

In a first step, to investigate a possible interference between the emission spectra of the two acceptor fluorophores, we measured in both channels the signals generated singularly by the antibody pairs 2B7/MW1 and 4C9/4C9. For this step, we analyzed brain homogenates of 11-week-old WT and R6/2 mice in the presence or absence of the antibodies (Figures 5A and 5B). Since no bleed-through of the two channels was detected, we successfully applied the duplex readout for determining soluble and aggregated mHtt by combining the two pairs of labeled antibodies in the same sample (Figure 5C). Importantly, the readout signals for soluble and aggregated mHtt displayed an overlapping linear range, allowing for a simultaneous quantitative duplex readout for both forms of the protein (Figure S7). In summary, we have developed and validated a duplex assay using the 2B7 Tb-MW1 d2 combined with the 4C9 Tb-4C9 Alexa antibody pair for detection of soluble and aggregated mHtt in biological samples.

Disease Progression-Related Changes in Soluble and Aggregated mHtt Protein Levels in R6/2 and *Hdh*Q150 Tissue

We proceeded to use the validated duplex TR-FRET assay for investigating the progression of soluble and aggregated mHtt protein in multiple tissues isolated from R6/2 mice at 5 or 11 weeks of age. We observed an age-dependent decrease in soluble mHtt correlating with an increase in aggregated mHtt in brain, muscle, and liver (Figure 6 and Table S1). Notably, in the testes, ear lobe, and spleen, while we were able to detect high levels of soluble mHtt, we did not observe any age-related changes in soluble levels nor any noticeable aggregation.

Having validated the successful application of the TR-FRET readouts in R6/2 mice, we asked ourselves whether we could also apply our methods to a milder HD mouse model. We therefore assessed the age-dependent soluble and aggregated mHtt signal development in cortical and striatal homogenates of 2- to 10-month-old heterozygote *Hdh*Q150 mice which express one

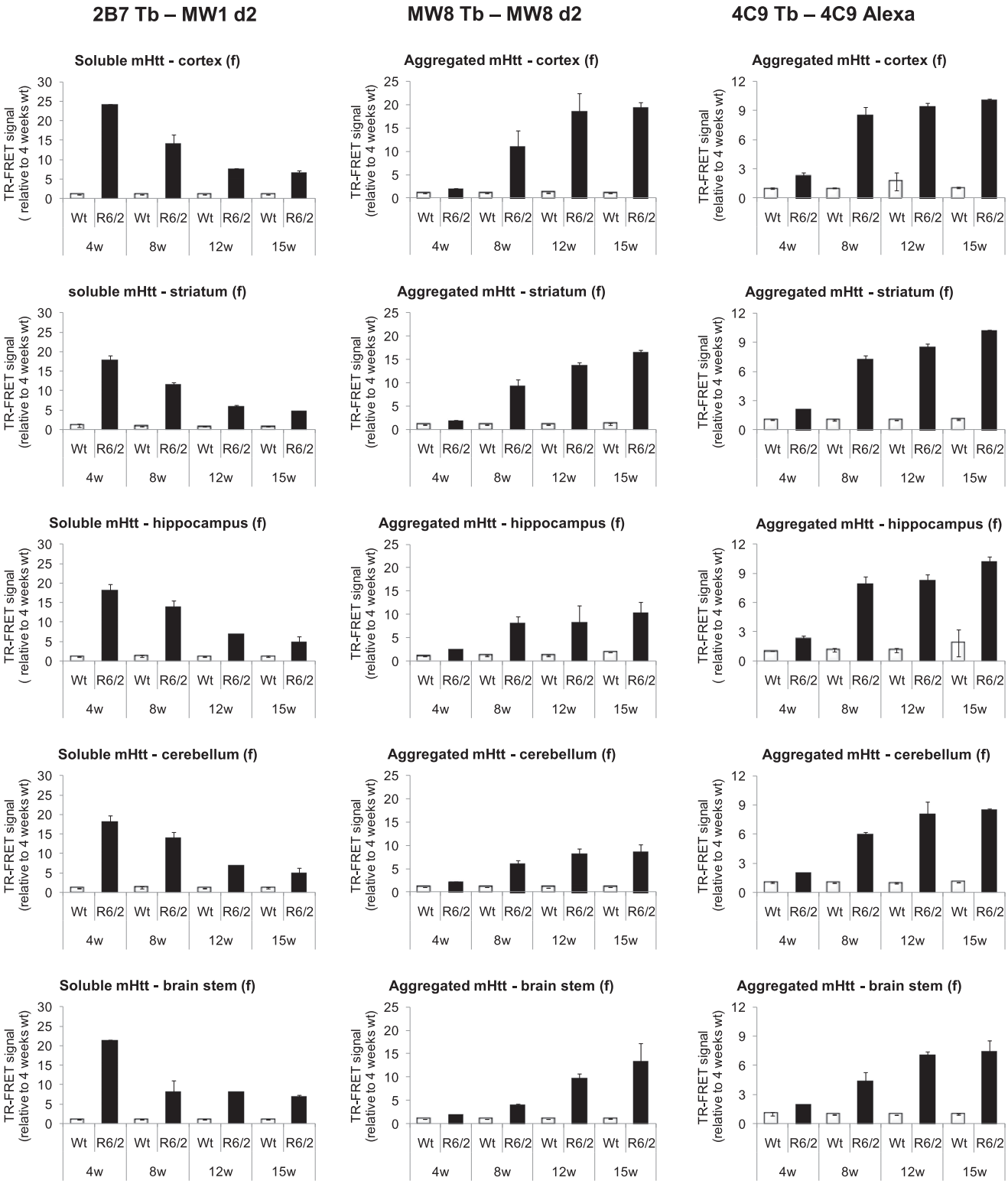

Figure 4. TR-FRET Assay Detects Age- and Disease-Progression Caused Changes in Soluble and Insoluble mHtt Protein Levels in WT and R6/2 Mouse Brain Regions

Homogenates from different brain regions from WT and R6/2 female mice have been analyzed to detect soluble (2B7/MW1) and aggregated mHtt (4C9/4C9; MW8/MW8) at different ages (4, 8, 12, and 15 weeks). All regions analyzed showed a correlation between the decrease over time of soluble mHtt signal and the progressive increase of the pool of aggregated mHtt. The cerebellum shows a lower aggregation load when analyzed with the MW8 antibody but not with the 4C9. Error bars = SD. See also Figure S5.

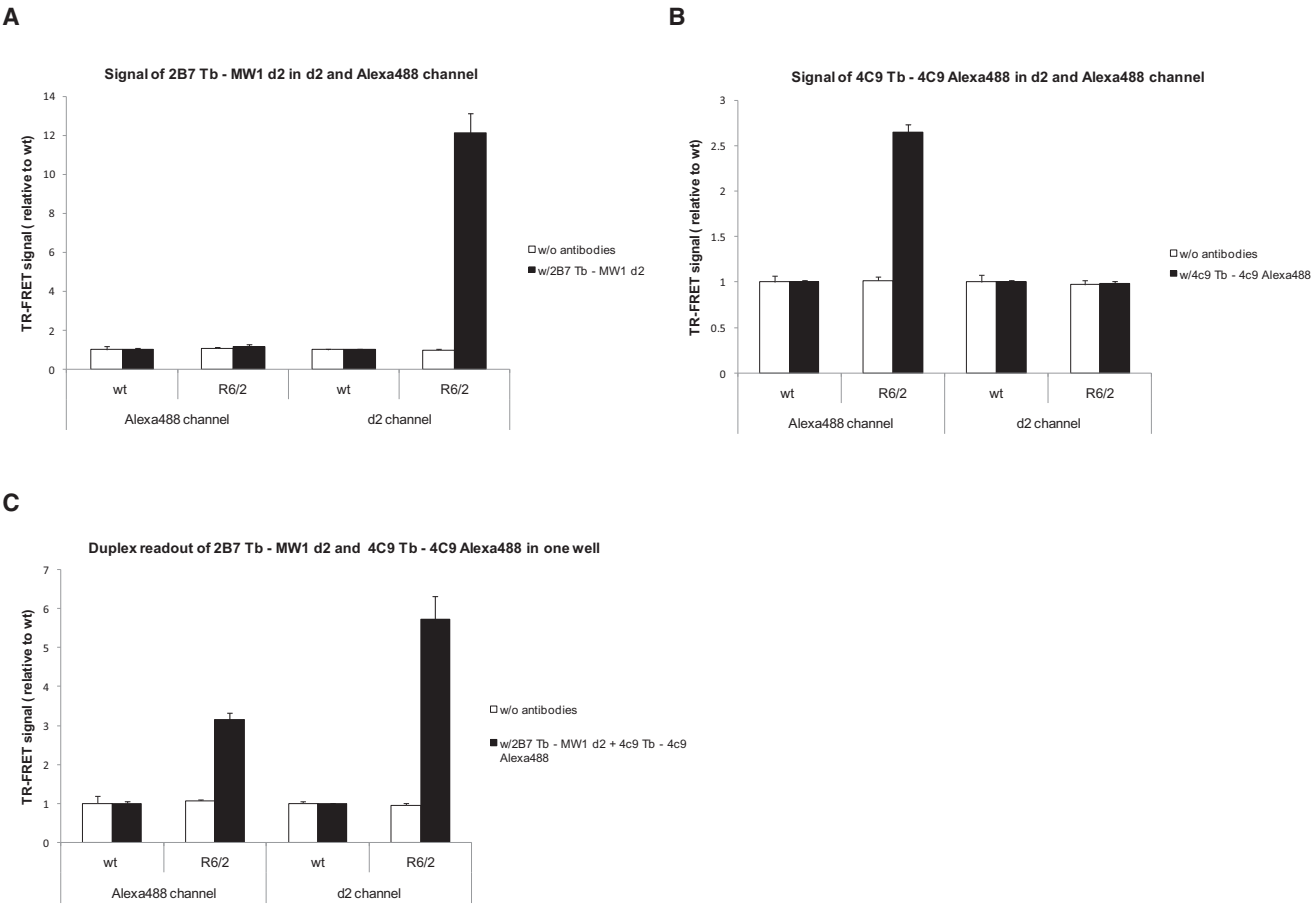

Figure 5. Signal Intensity Analysis for the Two Readout Channels Used to Quantify Soluble mHtt (2B7 Tb-MW1 d2 = d2 Channel) and Aggregated mHtt (4C9 Tb-4c9 Alexa = Alexa488 Channel)

(A and B) Signal measurement of the two readout channels analyzing 0.5 μg protein of 11-week-old WT or R6/2 mouse brain with or without addition of 2B7 Tb-MW1 d2 antibody (A) and with or without addition of 4C9 Tb + 4C9 Alexa antibody (B) reveals no signal bleed-through of one measurement into the other readout channels enabling a homogeneous duplex quantification of soluble and aggregated mHtt.

(C) Duplex quantification of soluble mHtt and aggregated mHtt in brain homogenates of 8-week-old WT or R6/2 mice using 1 μl assay buffer containing 1 ng 2B7 Tb, 10 ng MW1 d2, 1 ng 4C9 Tb, and 10 ng 4C9-Alexa were added to 0.5 μg brain protein in 5 μl brain homogenization buffer in a 384-low volume well. All graphs: n = 3; background signal = 0.5 μg BSA in brain homogenization buffer. Error bars = SD.

See also Figures S6 and S7.

allele of endogenous full-length mHtt with 150 glutamines. Similar to the data obtained from analysis of R6/2 brain, we observed an inverse correlation of soluble and aggregated mHtt signal in both brain regions and sexes using 2B7/MW1 and MW8/MW8 (Figure 7 and Figure S8). Use of the 4C9/4C9 assay in this model was precluded by the fact that this antibody recognized the human-specific proline-rich region of Htt which is absent in mouse Htt (data not shown). This result confirmed the value of the assays for quantification of two distinctive conformations of mHtt and their inverse correlation in a physiologically more relevant animal model of HD.

DISCUSSION

We have developed a simple and ultrasensitive duplex TR-FRET assay to simultaneously quantify nontagged soluble and aggregated mHtt in as little as 5 μl biological sample material.

Coupling the TR-FRET assay for insoluble mHtt aggregates with the 2B7/MW1 TR-FRET assay for soluble protein, we were able to monitor both conformational forms of the protein in solution. Moreover, the use of the polyQ-specific MW1 antibody resulted in a ~10-fold higher signal intensity for mHtt over WT Htt protein within the polyQ length ranges normally found in human alleles and an even more pronounced signal specificity for mHtt for polyQ lengths commonly used in animal models of the disease (Q7-Q18 for WT Htt, >Q100 for mHtt). This allowed us to identify dynamics occurring specifically in the mutant, pathogenic form of the soluble Htt and enabled us to investigate its relation with its aggregated pool also in presence of WT protein.

By combining the TR-FRET assay with SEC, we could show the specificity of our different assay readouts for distinct mHtt subpopulations in brain homogenates of HD mice. The specificity for a subset of small and large mHtt aggregates will help to identify and test mHtt aggregate modifiers and distinguish at

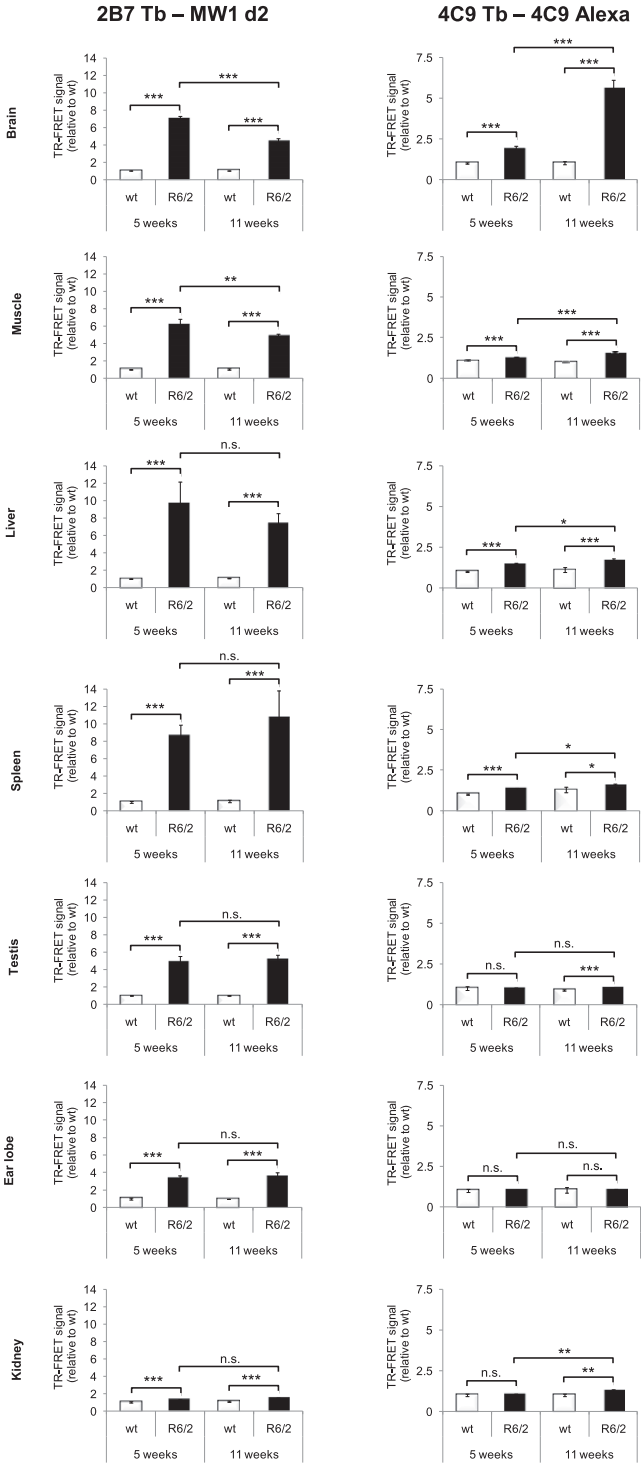

Figure 6. TR-FRET Duplex Assay Detects Age- and Disease-Progression Caused Changes in Soluble and Insoluble mHtt Protein Levels in WT and R6/2 Peripheral Tissue Homogenates

Tissues homogenates from WT and R6/2 mice of 5 and 11 weeks of age (n = 3) were analyzed using the TR-FRET duplex assay. A total of 0.5 μg of protein homogenate in 6 μl final volume per 384-well were analyzed to detect soluble mHtt (2B7/MW1) and insoluble aggregated mHtt (4C9/4C9). An age-dependent decrease in soluble mHtt correlating with an increase in aggregated mHtt is detected in R6/2 mouse brain, muscle, and liver. No significant changes in levels of aggregated mHtt or soluble mHtt levels were detectable in R6/2 mouse testis, ear lobe, spleen, and kidney. Error bars = SD. *p < 0.05; **p < 0.01; ***p < 0.001.

See also Tables S1 and S2.

what stage (early or late) they could be effective. Interestingly, the combination of SEC and TR-FRET showed that the heterogeneity of mHtt subpopulations did not change over time, but the relative abundance of individual mHtt aggregates did. Our analysis of nontagged mHtt expressed in in vivo HD models led to observations similar to those of previous works in which distinct species of GFP-tagged mHtt in in vitro systems were identified (Olshina et al., 2010), even though mHtt aggregation in cell culture may differ fundamentally from in vivo-generated aggregates in brain, as the neuronal context may lead to pathogenic interactions that still need to be identified.

The ratio of the progressive decrease of soluble mHtt at around 300 kDa with a progressive increase in the aggregated species at around 950 kDa can be monitored and set in direct relation. This is important in order to analyze potential biological activity (e.g., toxicity) of the mHtt aggregates. Interestingly, both MW8/MW8 and 4C9/4C9 detect high molecular weight aggregates as expected, but MW8/MW8 also recognized a smaller mHtt aggregate species in young animals. It is likely that MW8 detects aggregate precursors (oligomers) that disappear with age once large mHtt aggregates are formed. These oligomers may be prone to being folded into larger aggregates, indicating a regulated mechanism of inclusion body formation in cells. With the SEC purification together with the purity characterization by TR-FRET established, it will be interesting to test the biological activity and toxicity of these different mHtt species in future studies.

It has been previously shown that there is an inverse correlation between aggregated and soluble mHtt levels in R6/2 mouse brain (Sathasivam et al., 2010; Weiss et al., 2009; Woodman et al., 2007). Analyzing multiple brain regions isolated from R6/2 mice at different ages, we confirmed the previous observations and validate the specificity and value of the TR-FRET assay to provide a more detailed description of the changes occurring in soluble and aggregated Htt over time. While different regions of the brain contained comparable levels of soluble mHtt, higher amounts of aggregated protein were detected in the striatum and cortex over the cerebellum, brain stem, and hippocampus, in line with earlier findings (Sathasivam et al., 2010). Interestingly, these differences were only apparent when using the MW8/MW8 but not the 4C9/4C9 combination, further indicating that MW8 could recognize different aggregates species.

Combining the detection of soluble and aggregated mHtt in a duplex assay with high specificity for both mHtt forms, we were able to measure and compare both pools of the protein in brain and peripheral tissues from R6/2 mice. In all samples analyzed where an age-dependent decrease in soluble mHtt was observed, we detected a strong correlating progressive increase in the aggregated pool. These results suggest a mechanistic link between the mHtt pools, most likely through progressive recruitment of soluble mHtt into aggregates.

In contrast to in vitro aggregation studies in which clear concentration dependent aggregation kinetics of mHtt were observed (Chen et al., 2002; Scherzinger et al., 1999), our

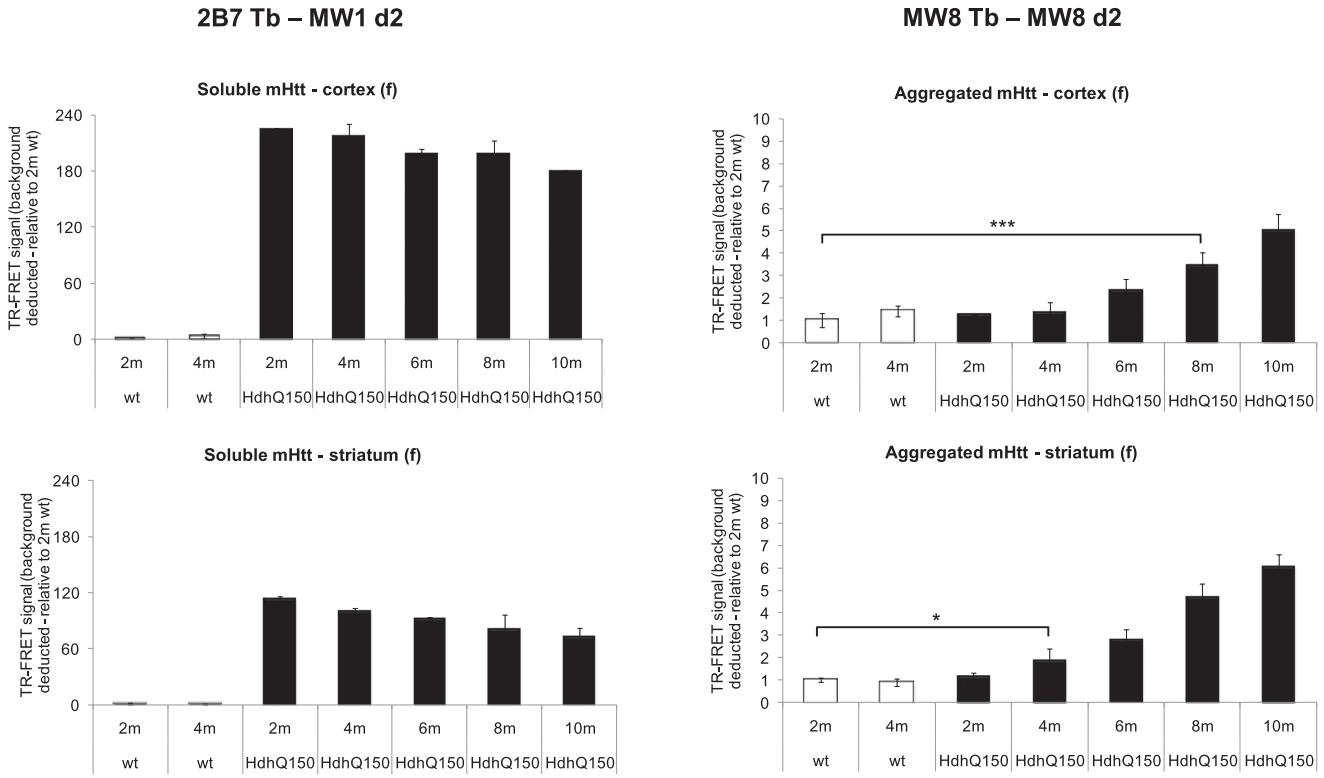

Figure 7. TR-FRET Detection of Changes Caused by Age and Disease Progression in Soluble and Insoluble mHtt Protein Levels in WT and Heterozygous *Hdh* Q150 Brain Regions

Cortical and striatal homogenates from WT and heterozygous *Hdh* Q150 female mice at different ages (2, 4, 6, 8, and 10 months) were analyzed with 2B7/MW1 (soluble mHtt) and MW8/MW8 (aggregated mHtt) TR-FRET (n = 3 per age). Both brain regions showed a correlation between a decrease of soluble mHtt signal and a progressive increase of aggregated mHtt over time. Error bars = SD. *$p < 0.05$; ***$p < 0.001$.
See also Figure S8 and Table S2.

findings indicate that the amount of intracellular soluble mHtt does not always correlate with its propensity to aggregate in a cell. For example, the testes contain high amounts of soluble mutant Htt protein, but no aggregates were detected. Other proliferating tissues such as the liver displayed expression levels of soluble mutant Htt similar to those seen in the testes but were characterized by age-dependent aggregate formation. This discrepancy in different tissues suggests that different proliferation rates may influence the propensity to develop aggregates by diluting mHtt below the threshold needed for aggregation. Of note, previous works have reported that the testes are highly degenerative in R6/2 mice and HD patients in absence of aggregates (Moffitt et al., 2009; Sathasivam et al., 1999; Van Raamsdonk et al., 2007). In light of the ongoing debate about mHtt aggregate toxicity, these observations raise the intriguing possibility that the pathogenic mechanism could be different in the context of different tissues. Importantly, this would also imply that treatment attempts should be aimed not solely at the reduction of aggregates, but also at upstream mechanisms to ameliorate the full spectrum of mHtt pathology.

The detection of mHtt aggregates in 4-month-old heterozygote *Hdh*Q150 mice using the MW8/MW8 assay highlights the sensitivity of the method. Interestingly, it has been recently reported that MW8 is directed against a neo-epitope at the C terminus of Exon1 (Landles et al., 2010). This could indicate the presence of a pure Exon1 population in this full-length mHtt model, responsible for the aggregation process and specifically detectable with this antibody. The possibility to specifically discriminate the quantitative levels of soluble and aggregated pathogenic protein levels in heterozygote animals, suggests the feasible translation of the immunoassay to the heterozygote HD patient population characterized by the presence of both soluble WT and mutant Htt forms, with the perspective to monitor changes during disease progression in human samples.

A limitation in our TR-FRET assays—as in any immunodetection method—is that the antibodies require their respective epitopes to be sufficiently exposed on the aggregate surface. Each assay may thus be specific for a subpopulation of aggregates. In addition, as larger aggregates have a lower surface to volume ratio than smaller aggregates, the TR-FRET signal intensity for large aggregates may be underrepresented in a heterogeneously sized pool. These limitations could be possibly overcome by further characterization of MW8 and 4C9 affinities to different aggregates populations. In addition, a better understanding of different aggregates populations measured by TR-FRET assays with specific antibodies could allow for a careful comparison to other technologies (such as Seprion ELISA) and design of experimental conditions to characterize changes occurring during disease progression or in response to treatment.

In conclusion, we developed, to our knowledge, novel assays that are at the same time sensitive, efficient, simple, and highly precise for quantification of aggregated and soluble mHtt. We made use of our assays to characterize and quantify the inverse correlation between those two conformational states of the protein in different in vitro and in vivo HD models. The simplicity of the assay protocol coupled with the efficient quantification allows for the use of the method in high-throughput screenings to identify modulators of the aggregation process, as well as in the evaluation of translational models of HD.

The research pursued in this study supports the correlation between decrease of soluble and increase of aggregated mHtt with disease progression in different HD models. Importantly, the ability to measure this tight relationship of the two mHtt conformational pools over time could yield novel insights for the debate of mHtt toxicity in HD.

SIGNIFICANCE

One of the key questions in the field of protein misfolding diseases is how to improve the ability to quantitatively measure protein aggregation and its various phases in vivo. This question is of particular importance for neurodegenerative disorders such as Huntington's disease (HD), Parkinson's disease (PD), or Alzheimer's disease (AD), in which aggregates have the chance to accumulate over decades in a postmitotic neuronal environment.

In this study, we present, to our knowledge, a new approach based on immune time-resolved Förster resonance energy transfer (TR-FRET) to simultaneously monitor endogenous soluble and aggregated nontagged disease proteins in biological tissue samples in a microtiter format.

Using this method, we could demonstrate, in samples from two different models of HD, that the progressive decrease of the soluble mutant huntingtin correlates with an increase of the aggregated fraction, suggesting a tight mechanistic link between the two forms of the protein. The sensitivity and simplicity of the method allowed us to address an open biological question in the HD field. Finally, the principle of this method can be applied to other diseases such as AD and PD. Our findings will thus help to elucidate whether an inverse correlation between soluble and aggregated protein species is a common pathological feature in neurodegenerative disorders.

EXPERIMENTAL PROCEDURES

Antibodies

MW1 and MW8 antibodies were developed by Paul Patterson (Ko et al., 2001) and obtained from the Developmental Studies Hybridoma Bank developed under the auspices of the NICHD and maintained by The University of Iowa, Department of Biological Sciences (Iowa City, IA). Generation and characterization of 2B7 was described previously (Weiss et al., 2009). 4C9 antibody was raised against the human polyproline region in exon1 of the huntingtin protein. Generation and characterization of β1 antibody was described previously (Paganetti et al., 1996).

Tissue Homogenization and Aggregates Ultracentrifugation

Crude tissue homogenates were prepared by homogenization in 10 volumes (w/v) of PBS + 1% Triton X-100 + Complete Protease Inhibitor (Roche, Switzerland) using preCellys tubes (Precellys) and two lysis cycles of 10'' at 6,000 rpm. Total homogenate protein concentration was determined with BCA assay (Thermo Scientific).

For the generation of soluble and insoluble, aggregates mutant huntingtin fractions, 1 ml R6/2 and WT brain tissues (~100 μg) were homogenized using a dounce homogenizer in PBS 1% Triton X-100 and centrifuged at 13,000 rpm for 5 min. A total of 100 μl supernatant was kept to be analyzed with AGERA (Start fraction), while 500 μl was subsequently ultracentrifuged at 80,000 × *g* for 90 min. The resulting supernatant was transferred to a fresh tube (Supernatant fraction). Pellet was resuspended and washed with lysis buffer. After a final ultracentrifugation step at 80,000 g, the pellet was resuspended in 500 μl lysis buffer (Pellet fraction). The three fractions were analyzed in parallel with AGERA and TR-FRET for the detection of soluble and aggregated Htt.

Agarose Gel Electrophoresis for Resolving Aggregates

Biochemical aggregate detection was performed using Agarose Gel Electrophoresis for Resolving Aggregates (AGERA) assay as previously described (Weiss et al., 2008). Briefly, 1.8 g agarose was dissolved in 100 ml 375 mM Tris HCl (pH 8.8) by boiling in a microwave. SDS was added to a final concentration of 0.1% and gels were poured. A total of 50 μg of homogenates was loaded per lane. AGERA gel was run at 100 V in Tris Glycine SDS Running Buffer (Invitrogen). The gel was then blotted at 15 V for 1 hr on a polyvinylidene fluoride membrane (Immobilon-P, Millipore), blocked with 5% milk for 1 hr at room temperature and incubated overnight with primary antibody, used at a concentration of 1.5 μg/ml in 2% milk diluted in Tris-buffered saline (TBS) + 0.1% Tween. After washing, membranes were incubated for 1 hr with anti-mouse secondary antibody 1:10,000 in 2% milk diluted in TBS + 0.1% Tween and developed using enhanced chemiluminescence (ECL) (GE Healthcare).

Aggregate Immunoprecipitation

R6/2 homogenates from 8-week-old mice were spun for 5 min at 13,000 rpm. A total of 300 μg total protein was incubated overnight at 4°C with 2 μg of antibody (4C9, MW8, 2B7, MW1, and β1) or control (G-Sepharose beads). Next, 15 μl G-sepharose beads equilibrated in lysis buffer were added to the samples and incubated 30 min at 4°C. Beads were subjected to three cycles of pelleting at 13,000 rpm for 30 s and washing with lysis buffer. A total of 20 μl loading buffer was added to the dried beads, and the samples were resolved on AGERA blot and detected with MW8.

Formic Acid Treatment and Filter Trap Assay

Brain homogenates from 8-week-old R6/2 mice were ultracentrifuged for 1 hr 30 min at 80,000 × *g*. The pellet was resuspended either with PBS or with 100% formic acid (Sigma) and incubated for 30 min at 37°C shaking in order to dissolve the insoluble mHtt aggregates (Hazeki et al., 2000). After neutralization to pH 7.0 with NaOH, the samples were analyzed via filter trap assay and TR-FRET. The filter trap assay was performed using cellulose acetate membrane with pores of 0.2 μm diameter (Whatman). The membrane was blocked for 1 hr with 5% milk and incubated overnight with 4C9 and MW8 antibodies at a concentration of 1.5 μg/μl in 2% milk diluted in PBS + 0.1% Tween. The signal was detected with ECL (GE Healthcare) after 1 hr incubation of the membrane with secondary antibody 1:10,000.

Purification of huntingtin Protein

The huntingtin-GST fusion protein coding sequences were cloned into pGEX-6P vectors. Recombinant plasmids were transformed into *E. coli* BL-21 by heat shock, and production of huntingtin protein fragments was induced with 0.1 mM isopropyl-1-thio-D-galactopyranoside at 16°C and 200 rpm overnight. After lysis of bacteria by sonication, GST fusion proteins were captured with Glutathione Sepharose 4B beads (GE Healthcare). The huntingtin protein fragments were cleaved from GST tags by incubating beads overnight at 4°C with PreScission Protease enzyme (GE Healthcare). Purified fusion proteins were then dialyzed against PBS with 1% Tween 20 and stored at −80°C until further use. Q16, Q19, Q22, Q42, Q49, and Q55 huntingtin proteins were produced, each containing the N-terminal sequence of huntingtin protein with 548 amino acids and a polyglutamine repeat of the indicated length.

TR-FRET for Soluble and Insoluble huntingtin Detection

Antibody labeling with Tb, d2, and Alexa fluorophores was performed by CisBio Bioassays. TR-FRET detection of soluble mutant huntingtin protein

in a singlex readout was performed as described (Weiss et al., 2009). In brief, 5 μl tissue homogenate sample was transferred to low-volume wells of white 384-microtiter plates (Greiner Bio-One, Monroe, NC). A total of 1 μl detection buffer (50 mM NaH_2PO_4, 400 mM NaF, 0.1% BSA, and 0.05% Tween + antibody mix) was added, with the final antibody amount per well for soluble mutant huntingtin detection being 1 ng 2B7-Tb + 10 ng MW1-d2. TR-FRET readout was performed with an EnVision Reader (PerkinElmer, Waltham, MA). After the excitation of the donor fluorophore Tb at 320 nm and a time delay of 100 μs, the resulting Tb and d2 emission signals were read at 620 nm and 665 nm, respectively.

Single TR-FRET detection of insoluble, aggregated mHtt was performed either by using MW8 antibody labeled with Tb (donor) or d2 fluorophores (acceptor), or by 4C9 antibody labeled with Tb (donor) or Alexa fluorophore (acceptor). TR-FRET protocol was similar to the one used for soluble mutant huntingtin with the following modifications: when using Alexa-labeled 4C9 antibody as an acceptor antibody, Alexa-specific emission signal was quantified at 520 nm. Duplex TR-FRET assay for simultaneous quantification of soluble and aggregates FR-TRET was performed by addition of 1 μl of 1 ng 2B7-Tb + 10 ng MW1-d2 and 1 ng 4C9-Tb + 10 ng 4C9-Alexa containing antibody mix per well.

Animal Models

Heterozygous R6/2 mice (Mangiarini et al., 1996) and heterozygous *Hdh*Q150 knock-in mice (Lin et al., 2001) were obtained from the laboratory of G. P. Bates. R6/2 were on a mixed C57BL/6 × CBA/Ca background. The colony was maintained by breeding them with B6 × CBA/CaF1 females. *Hdh*Q150 mice were maintained on a C57BL/6J background. The offspring were genotyped via PCR using DNA obtained from ear punches. The animals were housed in a temperature-controlled room that was maintained on a 12 hr light/dark cycle. Food and water were available ad libitum. Animals were sacrificed by decapitation in deep isoflurane narcosis. Tissues were then collected immediately and were snap-frozen on a metal plate placed on dry ice. All experiments were carried out in accordance with local guidelines for the care and use of laboratory animals.

Analysis of Soluble and Insoluble mHtt Aggregates by SEC

Analysis of mHtt Aggregates in the Supernatant by SEC and TR-FRET

For soluble fractions, half brain tissues from R6/2 were homogenized with Precellys according to the manufacturer instructions in 500 μl of sample buffer (1% Triton X-100 in PBS, Complete Protease Inhibitor (Roche) and PhosSTOP phosphatase inhibitor cocktail (Roche)) and finally sonicated for 10 s. Brain extracts were then clarified by ultracentrifugation for 30 min at 100,000 × *g*. Supernatant was filtered through a 0.45 μm membrane and fractionated by SEC on a Superdex 200 10/300 column. All of the SEC experiments were performed at 4°C with a flow rate of 0.5 ml/min. The elution was one column volume. The total protein loaded on the column were 1.7 mg in a sample volume of 500 μl. Protein standards with 0.5% Triton X-100 in PBS were used to estimate the size of Htt aggregatess (standard data not shown). Fractions (250 μl volume/fraction) were collected in a 96-well plate format, and 10 μl from each well was applied for TR-FRET measurement with indicated antibody combination.

Analysis of mHtt Aggregates in the Pellet by TR-FRET

For insoluble fractions, pellets from R6/2 brain homogenate obtained by centrifugation at 100,000 × *g* (density separation) were washed once (PBS + 1% Triton X) and resuspended in 2% Triton X-100 in PBS. A total of 10 μl suspension was assayed to TR-FRET measurement with indicated antibody combinations.

Primary Neuronal Cultures

Animals were maintained in accordance with Duke University Medical Center Institutional Animal Care and Use Committee guidelines (approval #A248-08-09). Cortico-striatal cocultures were prepared as described (Kaltenbach et al., 2010). Briefly, striata and cortices were dissected from embryonic day 18 rat brains and dissociated separately. A total of 5 × 10^6 cells were counted and transfected (Nucleofector, Lonza) with plasmids expressing Htt exon1 fragment carrying either 73 or 8 CAG expansion. Neurons were plated onto 96-well plates containing previously isolated astroglia feeder layers (2,000 cells/well) and then cultured in Neurobasal media (Invitrogen) supplemented with 5% fetal calf serum (Sigma-Aldrich), 2 mM glutamine (Glutamax, Invitrogen), 10 mM potassium chloride, and 5 μg/mL gentamicin at 37°C in 95% 0_2/5%CO_2. Brain-derived neurotrophic factor (Sigma) was diluted in Neurobasal media, added to the neurons immediately after plating, and replenished every other day until analysis. For TR-FRET analysis, cells were resuspended in lysis buffer (PBS + 1% Triton X-100 + Complete Protease Inhibitor tablet, Roche), shaken vigorously for 30 min at 4°C, and then stored at −80°C.

Statistics

Unless otherwise indicated, the data in the graphs correspond to the average of TR-FRET signals relative to the WT samples, and the bars are representative of the SD among the replicates. Significance was calculated using a two-tailed unpaired Student t test. Detailed p values for all graphs are shown in Table S2.

SUPPLEMENTAL INFORMATION

Supplemental Information includes eight figures and two tables and can be found with this article online at doi:10.1016/j.chembiol.2011.12.020.

ACKNOWLEDGMENTS

This work was supported by a European Commission Marie Curie Initial Training Network (215618) Fellowship (B.B.) and the CHDI Foundation (M.S., A.Z., G.P.B., D.C.L., and L.S.K.). B.B., S.G., D.A., D.M., G.P.L. and A.W. are employees of Novartis Pharma AG. P.P. is an employee of AC Immune. B.B., P.P., and A.W. designed and conceived the experiments. B.B. characterized the method and performed the TR-FRET experiments on R6/2 peripheral tissues. S.G performed the TR-FRET experiments on R6/2 brain regions and *Hdh*Q150 mice. D.M., G.P.L., and A.W. designed and performed the SEC experiments. L.S.K. and D.C.L. designed and performed the experiments with rat primary neuronal cultures. M.S. and A.Z. produced and analyzed the purified huntingtin proteins. D.A. collected the peripheral tissues from R6/2 mice. D.S. and G.P.B. provided the tissues from R6/2 and *Hdh*Q150 brain regions. B.B. and A.W. analyzed the data. B.B. and A.W. wrote the manuscript. P.P., D.C.L., G.P.L., L.S.K., and G.P.B. proofread the manuscript.

Received: July 28, 2011
Revised: November 22, 2011
Accepted: December 8, 2011
Published: February 23, 2012

REFERENCES

Chen, S., Berthelier, V., Hamilton, J.B., O'Nuallain, B., and Wetzel, R. (2002). Amyloid-like features of polyglutamine aggregates and their assembly kinetics. Biochemistry *41*, 7391–7399.

DiFiglia, M., Sapp, E., Chase, K.O., Davies, S.W., Bates, G.P., Vonsattel, J.P., and Aronin, N. (1997). Aggregation of huntingtin in neuronal intranuclear inclusions and dystrophic neurites in brain. Science *277*, 1990–1993.

El-Agnaf, O.M., Salem, S.A., Paleologou, K.E., Curran, M.D., Gibson, M.J., Court, J.A., Schlossmacher, M.G., and Allsop, D. (2006). Detection of oligomeric forms of alpha-synuclein protein in human plasma as a potential biomarker for Parkinson's disease. FASEB J. *20*, 419–425.

Fukumoto, H., Tokuda, T., Kasai, T., Ishigami, N., Hidaka, H., Kondo, M., Allsop, D., and Nakagawa, M. (2010). High-molecular-weight beta-amyloid oligomers are elevated in cerebrospinal fluid of Alzheimer patients. FASEB J. *24*, 2716–2726.

Gutekunst, C.A., Li, S.H., Yi, H., Mulroy, J.S., Kuemmerle, S., Jones, R., Rye, D., Ferrante, R.J., Hersch, S.M., and Li, X.J. (1999). Nuclear and neuropil aggregates in Huntington's disease: relationship to neuropathology. J. Neurosci. *19*, 2522–2534.

Hazeki, N., Nakamura, K., Goto, J., and Kanazawa, I. (1999). Rapid aggregate formation of the huntingtin N-terminal fragment carrying an expanded polyglutamine tract. Biochem. Biophys. Res. Commun. *256*, 361–366.

Hazeki, N., Tukamoto, T., Goto, J., and Kanazawa, I. (2000). Formic acid dissolves aggregates of an N-terminal huntingtin fragment containing an expanded polyglutamine tract: applying to quantification of protein components of the aggregates. Biochem. Biophys. Res. Commun. *277*, 386–393.

Hazeki, N., Tsukamoto, T., Yazawa, I., Koyama, M., Hattori, S., Someki, I., Iwatsubo, T., Nakamura, K., Goto, J., and Kanazawa, I. (2002). Ultrastructure of nuclear aggregates formed by expressing an expanded polyglutamine. Biochem. Biophys. Res. Commun. *294*, 429–440.

Hoffner, G., Island, M.L., and Djian, P. (2005). Purification of neuronal inclusions of patients with Huntington's disease reveals a broad range of N-terminal fragments of expanded huntingtin and insoluble polymers. J. Neurochem. *95*, 125–136.

Kaltenbach, L.S., Bolton, M.M., Shah, B., Kanju, P.M., Lewis, G.M., Turmel, G.J., Whaley, J.C., Trask, O.J., Jr., and Lo, D.C. (2010). Composite primary neuronal high-content screening assay for Huntington's disease incorporating non-cell-autonomous interactions. J. Biomol. Screen. *15*, 806–819.

Ko, J., Ou, S., and Patterson, P.H. (2001). New anti-huntingtin monoclonal antibodies: implications for huntingtin conformation and its binding proteins. Brain Res. Bull. *56*, 319–329.

Kuemmerle, S., Gutekunst, C.A., Klein, A.M., Li, X.J., Li, S.H., Beal, M.F., Hersch, S.M., and Ferrante, R.J. (1999). Huntington aggregates may not predict neuronal death in Huntington's disease. Ann. Neurol. *46*, 842–849.

Landles, C., Sathasivam, K., Weiss, A., Woodman, B., Moffitt, H., Finkbeiner, S., Sun, B., Gafni, J., Ellerby, L.M., Trottier, Y., et al. (2010). Proteolysis of mutant huntingtin produces an exon 1 fragment that accumulates as an aggregated protein in neuronal nuclei in Huntington disease. J. Biol. Chem. *285*, 8808–8823.

Legleiter, J., Mitchell, E., Lotz, G.P., Sapp, E., Ng, C., DiFiglia, M., Thompson, L.M., and Muchowski, P.J. (2010). Mutant huntingtin fragments form oligomers in a polyglutamine length-dependent manner in vitro and in vivo. J. Biol. Chem. *285*, 14777–14790.

Lin, C.H., Tallaksen-Greene, S., Chien, W.M., Cearley, J.A., Jackson, W.S., Crouse, A.B., Ren, S., Li, X.J., Albin, R.L., and Detloff, P.J. (2001). Neurological abnormalities in a knock-in mouse model of Huntington's disease. Hum. Mol. Genet. *10*, 137–144.

Lotz, G.P., Legleiter, J., Aron, R., Mitchell, E.J., Huang, S.Y., Ng, C., Glabe, C., Thompson, L.M., and Muchowski, P.J. (2010). Hsp70 and Hsp40 functionally interact with soluble mutant huntingtin oligomers in a classic ATP-dependent reaction cycle. J. Biol. Chem. *285*, 38183–38193.

Lunkes, A., Lindenberg, K.S., Ben-Haïem, L., Weber, C., Devys, D., Landwehrmeyer, G.B., Mandel, J.L., and Trottier, Y. (2002). Proteases acting on mutant huntingtin generate cleaved products that differentially build up cytoplasmic and nuclear inclusions. Mol. Cell *10*, 259–269.

Maat-Schieman, M.L., Dorsman, J.C., Smoor, M.A., Siesling, S., Van Duinen, S.G., Verschuuren, J.J., den Dunnen, J.T., Van Ommen, G.J., and Roos, R.A. (1999). Distribution of inclusions in neuronal nuclei and dystrophic neurites in Huntington disease brain. J. Neuropathol. Exp. Neurol. *58*, 129–137.

Mangiarini, L., Sathasivam, K., Seller, M., Cozens, B., Harper, A., Hetherington, C., Lawton, M., Trottier, Y., Lehrach, H., Davies, S.W., and Bates, G.P. (1996). Exon 1 of the HD gene with an expanded CAG repeat is sufficient to cause a progressive neurological phenotype in transgenic mice. Cell *87*, 493–506.

Mathis, G. (1993). Rare earth cryptates and homogeneous fluoroimmunoassays with human sera. Clin. Chem. *39*, 1953–1959.

Mitsui, K., Doi, H., and Nukina, N. (2006). Proteomics of polyglutamine aggregates. Methods Enzymol. *412*, 63–76.

Moffitt, H., McPhail, G.D., Woodman, B., Hobbs, C., and Bates, G.P. (2009). Formation of polyglutamine inclusions in a wide range of non-CNS tissues in the HdhQ150 knock-in mouse model of Huntington's disease. PLoS ONE *4*, e8025.

Myers, R.H. (2004). Huntington's disease genetics. NeuroRx *1*, 255–262.

Olshina, M.A., Angley, L.M., Ramdzan, Y.M., Tang, J., Bailey, M.F., Hill, A.F., and Hatters, D.M. (2010). Tracking mutant huntingtin aggregation kinetics in cells reveals three major populations that include an invariant oligomer pool. J. Biol. Chem. *285*, 21807–21816.

Paganetti, P.A., Lis, M., Klafki, H.W., and Staufenbiel, M. (1996). Amyloid precursor protein truncated at any of the gamma-secretase sites is not cleaved to beta-amyloid. J. Neurosci. Res. *46*, 283–293.

Ratovitski, T., Gucek, M., Jiang, H., Chighladze, E., Waldron, E., D'Ambola, J., Hou, Z., Liang, Y., Poirier, M.A., Hirschhorn, R.R., et al. (2009). Mutant huntingtin N-terminal fragments of specific size mediate aggregation and toxicity in neuronal cells. J. Biol. Chem. *284*, 10855–10867.

Sathasivam, K., Hobbs, C., Turmaine, M., Mangiarini, L., Mahal, A., Bertaux, F., Wanker, E.E., Doherty, P., Davies, S.W., and Bates, G.P. (1999). Formation of polyglutamine inclusions in non-CNS tissue. Hum. Mol. Genet. *8*, 813–822.

Sathasivam, K., Lane, A., Legleiter, J., Warley, A., Woodman, B., Finkbeiner, S., Paganetti, P., Muchowski, P.J., Wilson, S., and Bates, G.P. (2010). Identical oligomeric and fibrillar structures captured from the brains of R6/2 and knock-in mouse models of Huntington's disease. Hum. Mol. Genet. *19*, 65–78.

Scherzinger, E., Sittler, A., Schweiger, K., Heiser, V., Lurz, R., Hasenbank, R., Bates, G.P., Lehrach, H., and Wanker, E.E. (1999). Self-assembly of polyglutamine-containing huntingtin fragments into amyloid-like fibrils: implications for Huntington's disease pathology. Proc. Natl. Acad. Sci. USA *96*, 4604–4609.

Stack, E.C., Kubilus, J.K., Smith, K., Cormier, K., Del Signore, S.J., Guelin, E., Ryu, H., Hersch, S.M., and Ferrante, R.J. (2005). Chronology of behavioral symptoms and neuropathological sequela in R6/2 Huntington's disease transgenic mice. J. Comp. Neurol. *490*, 354–370.

The Huntington's Disease Collaborative Research Group. (1993). A novel gene containing a trinucleotide repeat that is expanded and unstable on Huntington's disease chromosomes. Cell *72*, 971–983.

Van Raamsdonk, J.M., Murphy, Z., Selva, D.M., Hamidizadeh, R., Pearson, J., Petersén, A., Björkqvist, M., Muir, C., Mackenzie, I.R., Hammond, G.L., et al. (2007). Testicular degeneration in Huntington disease. Neurobiol. Dis. *26*, 512–520.

Wang, C.E., Tydlacka, S., Orr, A.L., Yang, S.H., Graham, R.K., Hayden, M.R., Li, S., Chan, A.W., and Li, X.J. (2008). Accumulation of N-terminal mutant huntingtin in mouse and monkey models implicated as a pathogenic mechanism in Huntington's disease. Hum. Mol. Genet. *17*, 2738–2751.

Wanker, E.E. (2000). Protein aggregation and pathogenesis of Huntington's disease: mechanisms and correlations. Biol. Chem. *381*, 937–942.

Wanker, E.E., Scherzinger, E., Heiser, V., Sittler, A., Eickhoff, H., and Lehrach, H. (1999). Membrane filter assay for detection of amyloid-like polyglutamine-containing protein aggregates. Methods Enzymol. *309*, 375–386.

Weiss, A., Klein, C., Woodman, B., Sathasivam, K., Bibel, M., Régulier, E., Bates, G.P., and Paganetti, P. (2008). Sensitive biochemical aggregate detection reveals aggregation onset before symptom development in cellular and murine models of Huntington's disease. J. Neurochem. *104*, 846–858.

Weiss, A., Abramowski, D., Bibel, M., Bodner, R., Chopra, V., DiFiglia, M., Fox, J., Kegel, K., Klein, C., Grueninger, S., et al. (2009). Single-step detection of mutant huntingtin in animal and human tissues: a bioassay for Huntington's disease. Anal. Biochem. *395*, 8–15.

Weiss, A., Grueninger, S., Abramowski, D., Giorgio, F.P., Lopatin, M.M., Rosas, H.D., Hersch, S., and Paganetti, P. (2011). Microtiter plate quantification of mutant and wild-type huntingtin normalized to cell count. Anal. Biochem. *410*, 304–306.

Woodman, B., Butler, R., Landles, C., Lupton, M.K., Tse, J., Hockly, E., Moffitt, H., Sathasivam, K., and Bates, G.P. (2007). The Hdh(Q150/Q150) knock-in mouse model of HD and the R6/2 exon 1 model develop comparable and widespread molecular phenotypes. Brain Res. Bull. *72*, 83–97.